https://doi.org/10.5194/acp-2020-984
Preprint. Discussion started: 29 October 2020

Atmospheric Chemistry and Physics
Discussions

A revised mineral dust emission scheme in GEOS-Chem: improvements in dust simulations over China

Rong Tian[1], Xiaoyan Ma[1*], Jianqi Zhao[1]

[1]Collaborative Innovation Center on Forecast and Evaluation of Meteorological Disasters (CIC-FEMD)/Key Laboratory for Aerosol-Cloud-Precipitation of China Meteorological Administration, Nanjing University of Information Science & Technology, Nanjing 210044, China

Correspondence to: Xiaoyan Ma (xma@nuist.edu.cn)

Abstract：

Mineral dust plays a significant role in climate change and air quality, but large uncertainties remain in terms of dust emission prediction. In this study, we improved the treatments of dust emission process in a Global 3-D Chemical Transport model (GEOS-Chem) v12.6.0, by incorporating the geographical variation of aerodynamic roughness length (Z_0), smooth roughness length (Z_{0s}), soil texture, introducing Owen effect and Lu and Shao (1999) formulation of sandblasting efficiency α. To investigate the impact of the modifications incorporated in the model, several sensitivity simulations were performed for a severe dust storm during March 27, 2015 to April 2, 2015 over northern China. Results show that simulated threshold friction velocity is very sensitive to the updated Z_0 and Z_{0s} field, with the relative difference ranging from 10% to 60% compared to the original model with uniform value. An inclusion of Owen effect leads to an increase in surface friction velocity, which mainly occurs in the arid and semi-arid regions of northwest China. The substitution of fixed value of α assumed in original scheme with one varying with friction velocity and soil texture based on observations reduces α by 50% on average, especially over regions with sand texture. Comparisons of sensitivity simulations and measurements show that the revised scheme with the implement of updates provides more realistic threshold friction velocities and PM_{10} mass concentrations. The performance of the improved model has been evaluated against surface PM_{10} observations as well as MODIS aerosol optical depth (AOD) values, showing that the spatial and temporal variation of mineral dust are better captured by the revised scheme. Due to the inclusion of the improvement, average PM_{10} concentrations at observational sites are more comparable to the observations, and the average mean bias (MB) and normalized mean bias (NMB) values are reduced from -196.29μg m^{-3} and -52.79% to -47.72μg m^{-3} and -22.46% respectively. Our study suggests that the erodibility factor, sandblasting efficiency and soil-related properties which are simply assumed in the empirical scheme may lack physical mechanism and spatial-temporal representative. Further study and measurements should be conducted to obtain more realistic and detailed map of these parameters in order to improve dust representation in the model.

1 Introduction

Mineral dust is typically produced by wind erosion from regions with arid and semi-arid surfaces in the world and exerts significant impacts on the atmospheric radiation balance (Tegen et al., 1996; DeMott et al., 2010; Kumar et al., 2014; Saidou Chaibou et al., 2020a), climate (DeMott et al., 2003; Mahowald and Kiehl, 2003; Zhao et al., 2012; Chen et al., 2014; Chin et al., 2014), air quality (Giannadaki et al., 2014; Tian et al., 2019) and human health (Goudie, 2014; Tong et al., 2017). Dust emission process has been recognized as a leading contributor to dust aerosol loading. Global mineral dust particles are mainly emitted from North Africa, the Arabian Peninsula, Central Asia, East Asia, Australia and North

America, with East Asia (including the Gobi and Taklimakan deserts) accounting for ~20% of the global dust emission (Ginoux et al., 2004; Nagashima et al., 2016).

In order to properly reproduce dust emission process, many dust emission schemes have been developed and implemented in both global and regional chemical transport models (CTMs) (e.g., Marticorena and Bergametti, 1995; Lu and Shao, 1999; Alfaro and Gomes, 2001; Shao, 2001, 2004; Shao et al., 2011; Zender et al., 2003; Kok, 2011a, 2011b). Nevertheless, some intercomparison studies demonstrated that there are large discrepancies among different dust emission models (Uno et al., 2006; Todd et al., 2008; Huneeus et al., 2011; Su and Fung, 2015; Ridley et al., 2016; Chen et al., 2017; Chen et al., 2019; Ma et al., 2019; Wu et al., 2019; Saidou Chaibou et al., 2020b; Zhao et al., 2020). Ma et al. (2019) quantitatively evaluated the performance of three dust schemes in WRF-Chem, two schemes in both CHIMERE and CMAQ, and one scheme in CAMx during a dust episode over northern China. Large differences between observed surface PM_{10} concentrations and modelling results of each model were found. Among schemes in WRF-Chem, AFWA and UOC_Shao2004 are better correlated with observations compared to GOCART but tend to overestimate dust concentrations. Kang et al. (2011) compared the performance of three dust emission schemes in WRF-Chem over East Asia, showing that the difference of dust emission fluxes between three schemes ranges from an order of 10^1 to 10^2. Ridley et al. (2016) showed that the estimated global dust AOD vary by over a factor of 5 among four global models (including GEOS-Chem, WRF-Chem, CESM and MERRAero), and dust emissions across North Africa are overestimated while emissions from Asia and the Middle East are underestimated overall. An intercomparison of 14 CTMs as part of the Model Inter-Comparison Study for Asia (MICS-Asia) phase III project (Chen et al., 2019) showed that nearly all participant models underestimate PM_{10} levels and current CTMs have difficulty producing similar dust emissions when adopting different dust schemes.

The uncertainties in dust emission models can be attributed to a number of issues, such as threshold friction velocity, surface wind speed, soil texture, particle size distribution, other soil/surface parameters (e.g., soil moisture, vegetation cover, aerodynamic roughness length) and different physical mechanisms (Tegen, 2003; Zhao et al., 2013; Liu et al., 2018; Chen et al., 2019). Darmenova et al. (2009) conducted a detailed comparison between two schemes developed by Marticorena and Bergametti (1995) and Shao et al. (1996), indicating that wind friction velocity is a significant factor in simulating dust emission while the aerodynamic roughness length as well as vegetation cover may play an important role at higher wind speed. Many sensitivity experiments have been conducted and shown that the modeled threshold friction velocity can be modified by soil moisture (Cheng et al., 2008; Mokhtari et al., 2012; Gherboudj et al., 2015; Ju et al., 2018), soil texture (Menut et al., 2013; Gherboudj et al., 2015; Perlwitz et al., 2015a, 2015b; Kontos et al., 2018) and surface roughness (Cheng et al., 2008; Astitha et al., 2012; Menut et al., 2013), which in turn affects the predicted dust emission. In addition, a more accurate value of sandblasting mass efficiency (α) has been reported to be a crucial factor for a better performance of dust emission flux (Mokhtari et al., 2012; Klingmüller et al., 2018; Kontos et al., 2018; Ma et al., 2019).

Based on the above studies, it is necessary to take these key parameters, including soil-related properties and empirical input parameters, into fully consideration in a dust emission parameterization. Unfortunately, due to limited observations, many of these parameters are not well included in the model. For example, most dust models simply assume a constant values of aerodynamic roughness length and soil clay fraction (Ginoux et al., 2001; Tegen et al., 2002; Zender et al., 2003), ignoring the temporal and spatial variability of them, which may cause uncertainties to the estimated surface friction velocity and threshold friction velocity. During recent decades, with the development of observation technology, the detailed information on the surface characteristics appropriate for global and regional models have been provided (Laurent et al., 2005, 2008; Prigent et al., 2005, 2012; Shangguan et al., 2014; Perlwitz et al., 2015a, 2015b). Therefore, adopting more accurate and detailed soil datasets is expected to improve the dust model performance.

In this study, we present an improvement of the dust emission scheme in GEOS-Chem model by incorporating the updated soil texture and aerodynamic roughness length with spatial variability, Owen effect, drag partition correction factor as well as the updated formulation of sandblasting efficiency, which together significantly improve the prediction of dust emission flux and concentrations over China. The objective is to obtain more realistic surface friction velocity (u_*) and threshold friction velocity (u_{*t}) by considering the effect of the soil moisture, surface roughness and soil texture, thus improving the representation of dust emission in the model.

Section 2 gives a detailed description of GEOS-Chem model and the modifications of the improved scheme as well as numerical experiments and data description. Sensitivity results are compared in Section 3.1 to examine the impacts of the modifications. Section 3.2 presents the comparisons of the improved scheme and original version with observations, to evaluate the performance of the improved scheme. Uncertainties, limitations, and future improvements of the emission scheme are discussed in Section 3.3, followed by a summary in Section 4.

2 Model and measurements

2.1 Model description

The GEOS-Chem model is a global three-dimensional chemical transport model driven by assimilated meteorology. In this work, we use v12.6.0 of GEOS-Chem driven by GEOS-FP assimilated meteorological field with a spatial resolution of 0.25° × 0.3125° and 72 vertical levels for China region (15-55°N, 70-140°E) during the period of March 27, 2015 to April 2, 2015. The lateral boundary conditions is provided by a global simulation of 2° × 2.5°.

GEOS-Chem includes detailed atmospheric chemical mechanism and online aerosol calculations. In this work, we simulate the dust emission with a combination of the dust entrainment and deposition (DEAD) mobilization scheme (Zender et al., 2003) and Global Ozone Chemistry Aerosol Radiation and Transport (GOCART) source function. Dry deposition velocities for dust aerosols are computed with the gravitational settling scheme of Fairlie et al. (2007) and aerosol deposition scheme from Zhang et al. (2001). Wet deposition scheme, which includes scavenging in convective updrafts, as well as rainout and washout of soluble tracers, is described in Liu et al. (2001). Aerosol optical depth is derived online from aerosol concentrations with externally-mixed assumption using RH-dependent aerosol optical properties from Latimer and Martin (2019). Dust optics are from Ridley et al. (2012).

2.2 Improvement on the dust emission scheme in GEOS-Chem

The standard dust emission scheme in GEOS-Chem is based on a semi-empirical formulation developed by Zender et al. (2003) and is combined with GOCART source function (Ginoux et al., 2001). In this scheme, the vertical dust flux (F) is proportional to the horizontal saltation flux (Q_s), which is the function of surface friction velocity (u_*) and threshold friction velocity (u_{*t}):

$$F = (1 - A_s) S \alpha Q_s \tag{1}$$

$$Q_s = C_z \frac{\rho_{air}}{g} u_*^3 \left(1 - \frac{u_{*t}}{u_*}\right)\left(1 + \frac{u_{*t}}{u_*}\right)^2 \quad u_* > u_{*t} \tag{2}$$

where α is the vertical-to-horizontal flux ratio or sandblasting efficiency, based on the soil clay content (Marticorena and Bergametti, 1995). S is based on GOCART source function (see Fig. S1), also named as the soil erodibility factor, representing the grid cell fraction of the bare land suitable for mobilization. A_s is the fraction of snow-covered surface. C_z is the saltation constant (C_z=2.61).

According to the equation, u_{*t}, u_* as well as α are the key input parameters in the accurate prediction of dust emission flux. u_{*t} is used to describe the characteristics of soil and land surface condition, representing the resistance of surface to wind erosion. In the standard dust scheme, u_{*t} is calculated using a semi-empirical formulation as a function of air density and soil particle density (Iversen and White, 1982). Furthermore, two correction terms, including soil moisture correction (Fécan et al., 1999) and drag partition correction (Marticorena and Bergametti, 1995), are also applied to modify u_{*t}. It should be noted that in the original scheme, the drag partition correction term is eliminated.

u_* is a description of surface wind speed, which mainly depends on 10m wind speed taken from meteorological field assuming neutral stability (Bonan, 1996). Owen effect, which represents a positive feedback between saltation process and friction speed (Owen, 1964), is often adopted in models to modify u_*. However, Owen effect is eliminated in the original scheme.

Sandblasting efficiency α is parameterized according to the empirical relation described by Marticorena and Bergametti (1995) (MB95), which depends on the soil clay content (M_{clay}) and is restricted to $M_{clay} < 20\%$:

$$\alpha = 100e^{(134M_{clay}-6)ln10} \tag{3}$$

However, in the global model, α tends to be overly sensitive to M_{clay}. Due to this reason, a globally fixed value of $M_{clay} = 20\%$ is assumed in current model (Zender et al., 2003).

It should be noted that, some input parameters, data or formulations are quite simplified and need to be improved based on the original dust scheme described above. For example, the aerodynamic roughness length (Z_0), the smooth roughness length (Z_{0s}) as well as the mass fraction of clay in the soil (M_{clay}) are assumed as a constant uniformly, despite the fact that it may vary with time and location. As a result, the simulation of related processes, such as drag partition effect or soil moisture effect, may lack spatial representation. Therefore further modifications on these variables should be made in order to obtain more realistic dust emission. Fig. S2 presents the schematic diagram of the dust emission schemes in the standard model and the modifications incorporated in this study. The details of the parameterization options and required input parameters are presented in following sections.

2.2.1 Soil Type and Soil Texture Data

In the model, M_{clay} can have an impact on u_{*t} through modifying soil moisture correction term, thus influencing the modeled dust emission flux. The soil moisture correction term, defined as f_w, is parameterized according to Fécan et al. (1999), which accounts for the increase of u_{*t} with soil moisture content.

$$f_w = \begin{cases} 1 & w < w' \\ [1 + 1.21(w - w')^{0.68}] & w \geq w' \end{cases} \tag{4}$$

$$w'(\%) = a\left(0.0014{M_{clay}}^2 + 0.17M_{clay}\right) \tag{5}$$

where w is gravimetric soil moisture and w' is soil residual moisture.

With the increase of soil moisture, soil cohesion can be enhanced, particularly over regions with high clay content, thus inhibiting sandblasting process to some extent. However, as stated above, M_{clay} is assumed as a constant equal to 20% in the original scheme, which can cause uncertainty in dust prediction. In the improved scheme, we employ the gridded data of clay content from the Global Soil Dataset for use in Earth System Models (GSDE) (Shangguan et al., 2014), which is based on the Soil Map of the World and various regional and national soil databases. Fig. 1 shows the updated M_{clay} from Shangguan et al. (2014) with the horizontal resolution of 2° × 2.5° at the global scale. Compared to the original fixed value of 20%, the updated M_{clay} is generally lower in most of the dust source areas over East Asia.

2.2.2 Surface roughness length

The drag partition is used to describe the impact of roughness elements (such as rocks, pebbles, vegetation, etc.) on u_{*t}. According to Marticorena and Bergametti (1995), the roughness correction term, f_d, is a function of the aerodynamic roughness length Z_0 and the smooth roughness length (Z_{0s}):

$$f_d = 1 - \frac{\ln(\frac{z_0}{z_{0s}})}{ln\left[0.7\left(\frac{12255cm}{z_{0s}}\right)^{0.8}\right]} \tag{6}$$

where the required roughness lengths are set as the constant values of $Z_0 = 0.01$ cm and $Z_{0s} = 0.0033$ cm globally.

Z_0 represents the roughness length of the overlying non-erodible elements (solid obstacles, such as rocks), which transfers part of the wind momentum from the atmosphere to the surface, dissipating the shear force for particle saltation. Prigent et al. (2005) derived global aerodynamic roughness length in arid and semi-arid areas which are retrieved from the ERS-1 satellite measurements with a horizontal resolution of 0.25° × 0.25°. Here we apply the global monthly mean Z_0

https://doi.org/10.5194/acp-2020-984
Preprint. Discussion started: 29 October 2020

fields provided by Prigent et al. (2005) and then re-grid the map to 2° × 2.5° horizontal resolution for the incorporation into GEOS-Chem. As Fig. 2 shows, compared to the fixed constant assumed in the original version, the updated global Z_0 is generally higher. Over northern China, the Z_0 value ranges from approximately 0.01cm over desert regions to 0.07cm.

Z_{0s} characterizes the roughness length of the uncovered, bare erodible surface. Instead of setting Z_{0s} to a fixed value, some studies suggested that Z_{0s} can be estimated as 1/30 of the coarse-mode mass median diameter (MMD) of soil particles, which will provide more realistic representation of soil texture distribution (Marticorena and Bergametti, 1995; Laurent et al., 2006; Mokhtari et al., 2012). In the improved version, we adopt this empirical formula, based on updated soil texture classification (Mokhtari et al., 2012; Xi et al., 2015), to estimate Z_{0s}:

$$z_{0s} = MMD/30 \tag{7}$$

where MMD is the median diameter of the coarsest mode for various soil textures shown in Table 1. The corresponding Z_{0s} for different soil types are listed in Table 1 and its global distribution is shown in Fig. 3. The soil texture map is obtained based on the Harmonized World Soil Database (HWSD; http://www.iiasa.ac.at/Research/LUC/External-World-soil-database/HTML), which provides global sand, silt, and clay contents at 30 arc-second resolution. The soil texture dataset is re-gridded to 2° × 2.5° resolution, and then is applied to identify the global soil texture by using the United States Department of Agriculture (USDA) soil texture triangle (based on the amount of sand, clay, and silt contents; http://soils.usda.gov/technical/aids/investigations/texture/). There are 12 classes of soil defined by USDA. It can be seen from Fig. 4 that loam, sandy loam and clay loam, are the dominant soil types over China. Among them, sandy loam and loam occupy the major part of northwest China.

2.2.3 Sandblasting efficiency α

Sandblasting efficiency α is important in the dust emission calculation as it is used to convert the horizontal saltation mass flux to a vertical dust mass flux. In the original scheme, α is simply expressed as a function of M_{clay}, which is a fixed value of 20%. The assumption in the original scheme might cause uncertainty in modeled flux and make the spatial variation less representative (Mokhtari et al., 2012).

In order to reduce this uncertainty, a more physically-based function from Lu and Shao (1999) (LS99) is adopted in our study. Based on wind tunnel experiments carried out by Rice et al. (1996a, b), Lu and Shao (1999) derived the expression of α through theoretical calculation and some simplifications:

$$\alpha = \frac{C_\alpha g f \rho_b}{2p}(0.24 + C_\beta u_* \sqrt{\frac{\rho_p}{p}}) \tag{8}$$

where f is the fine particles content in the soil volume, p is soil plastic pressure, which represents the magnitude of the surface resistance (N m^{-2}), ρ_b and ρ_p are the bulk soil density and particle density, respectively, g is the gravitational acceleration (m s^{-2}), u∗ is friction velocity (m s^{-1}), and C_α and C_β are empirical constants. Among these parameters, the values of ρ_b and p depend upon different soil textures. Some studies (Kang et al., 2011; Foroutan et al., 2017; Ma et al., 2019) have implemented this formulation in the model and proposed the proper range of these parameters over different soil types.

Many measurements from laboratory experiments and field observations have demonstrated the close relationship between α and u_* (Gillette et al., 1997; Gomes et al., 2003; Rajot et al., 2003; Roney and White, 2006; Macpherson et al., 2008; Panebianco et al., 2016; Zhang et al., 2016). To improve the original scheme, we extract α from these measurements over different soil types, based on the expression of LS99, as depicted in Fig. 5 and Table 2.

2.3 Experiments design

Several sensitivity experiments (Table 3) are conducted to assess the model performance of the modifications in the improved scheme. Control is the control run with the dust emission scheme originally implemented by Fairlie et al. (2007). Sen_mclay, Sen_owen, Sen_ratio, Sen_drag and Sen_Z_0Z_{0s} are the same as the control run but including the modification of M_{clay}, Owen effect, sandblasting efficiency, drag partition effect and updated surface roughness length (Z_0 and Z_{0s}) respectively. Sen_all represents the simulation with the improved scheme which accounts for all the modification described above.

2.4 Measurements

The data used in this study includes the Moderate Resolution Imaging Spectrometer (MODIS) Level 3 AOD data, hourly observational data of surface PM_{10} concentration, and meteorological field taken from the Meteorological Information Comprehensive Analysis and Process System (MICAPS). The data used in this study is for the period of March 27, 2015 to April 2, 2015.

MODIS aerosol products are used to evaluate model results of AOD. MODIS AOD at 550 nm is obtained from the daily level-3 product from Aqua satellites (MYD08_D3, 1°×1° gridded data) and is combined with Deep Blue retrievals which can provide AOD over bright surfaces (i.e., desert regions).

Hourly surface observed PM_{10} concentration data, collected from about 1000 environmental monitoring stations maintained by Chinese Ministry of Environmental Protection (MEP; http://datacenter.mep.gov.cn), is used to validate the model performance of surface dust concentrations.

Meteorological fields of wind speed taken from the Meteorological Information Combine Analysis and Process system (Micaps) developed by the Chinese National Meteorological Center (NMC) are used for evaluation of wind field in the model. Fig. S3-S4 show that the 10m wind field used in the model scheme generally agree well with the Micaps observations over most sites. However, comparisons of averaged surface wind field between the model input and observations (Fig. S5) show that although the circulation patterns in the model are identical with the observations, surface wind speed in the model tend to be larger than observations, especially over western and northeastern Inner Mongolia.

3 Results and discussion

3.1 Sensitivity study

In order to assess the sensitivity of the dust emission to the modified input parameters or physical processes, several numerical experiments are conducted and compared. Fig. 6a presents the relative difference (%) of averaged u_{*t} during study period between these sensitivity simulations and the control run. The u_{*t} simulated by Control run are generally small, with values less than 0.3m/s (not shown). Wu et al. (2013) indicated that u_{*t} over source regions in northern China calculated by Zender et al. (2003) are generally lower (with values ranging from 0.2 to 0.25 m/s) than the measurement (with values ranging from 0.34 to 0.69 m/s) and the values calculated by Shao (2004), which is closer to the observations. The sensitivity simulations show that the update of M_{clay} in Sen_mclay can lead to higher u_{*t} over northern China and lower u_{*t} over southern China than the control simulation, which overestimates M_{clay} over northern China while underestimates it over southern China by setting M_{clay} to 20%. In northern China, particularly in arid and semi-arid regions, the updated M_{clay} will decrease the soil moisture threshold w' and increase soil moisture term f_w, thus leading to a slight increase in u_{*t} (with magnitude <10%). The inhibition of dust emission by surface roughness elements is not taken into account in the original scheme, i.e., f_d=1. Some studies (Darmenova et al., 2009; Menut et al., 2013) have demonstrated f_d as a function of Z_0 and Z_{0s}, implying that f_d increase with Z_0 and decrease with Z_{0s}. Compared to the fixed values used in the original scheme, updated Z_0 field used in Sen_ Z_0Z_{0s} are generally larger and updated Z_{0s} field are smaller. Therefore, f_d are increased significantly, particularly over the regions with non-erodible elements (larger Z_0). Result shows that u_{*t} is increased when considering the drag partition effect (increased by 10% in Sen_drag with constant Z_0 field), particularly with the updated Z_0 and Z_{0s} field (increased by 10%~60% in Sen_ Z_0Z_{0s}). In general, due to the inclusion of Z_0, Z_{0s} and M_{clay}, f_d and f_w are modified, which results in significant alteration in u_{*t} (ranging from -8%~72% in Sen_all) over China. It can be found that the modification of f_d due to updated Z_0 and Z_{0s} makes more contribution to the increase in

https://doi.org/10.5194/acp-2020-984
Preprint. Discussion started: 29 October 2020

u_{*t}.

Relative difference of u_* with respect to the control run are also compared in Fig. 6b. Considering Owen effect in Sen_owen leads to an increase in u_* by 0%~39%, especially over northwest China where surface wind is strong. Modeled u_* is obtained from u10m and Z_0 under neutral conditions (Bonan, 1996). It can be seen that updated Z_0 in Sen_ Z_0Z_{0s} can modify u_* by influencing the boundary-layer exchange properties. u_* over northern China is generally increased by 10%~22% with higher values of Z_0 in Sen_ Z_0Z_{0s}, while it is slightly decreased over Taklimakan and Gobi deserts. In Sen_all, modeled u_* is increased by 5%~50% over most parts of China.

Fig. 6c presents the percentage difference in terms of sandblasting efficiency α. In the original version, α is set as a uniformly constant value (around 0.04) due to the assumption of a fixed M_{clay}. In Sen_ratio and Sen_all, u_*-dependent-ratio following LS99, which varies with different soil texture according to observations, is adopted. On average, α is decreased by 50% with the modification in Sen_ratio and Sen_all. The largest reduction occur over regions with sand texture such as over Taklimakan and Gobi Desert.

As seen from Fig. 6d, the simulated dust emission flux (F) vary significantly among different experiments. Due to the inclusion of updated M_{clay}, soil moisture term increases in Sen_mclay, which leads to higher u_{*t} and lower F over most regions. Accounting for Owen effect in Sen_owen results in an increase in F of 0%~314%, particularly over northern part of Gansu Province and northwestern Inner Mongolia. A significant reduction in arid and semi-arid regions of northern China is caused by updated α (Sen_ratio). In Sen_drag and Sen_ Z_0Z_{0s}, F are influenced by -100% ~-4% and -100%~50% respectively as a result of the inclusion of f_d with constant Z_0 and updated Z_0, Z_{0s} respectively. Due to the combined effects of the modifications, F simulated by Sen_all is generally reduced over northern China, except in some regions of northwest China, where Owen effect plays a dominant role.

Four sites closer to dust source area or significantly influenced by dust-storms (Beijing, Huhehaote, Jiuquan and Kuele, locations shown in Fig. S1) are selected to evaluate the performance of control and sensitivity simulations. Comparisons of the modeled u_{*t} (Fig. 7) show that in all sites, modeled u_{*t} are increased in Sen_mclay, Sen_drag, Sen_ Z_0Z_{0s} and Sen_all, compared with the original model, with the highest u_{*t} simulated by Sen_all. Modeled u_{*t} increase from 0.22~0.25m/s in Control to 0.32~0.37m/s in Sen_all. The reported u_{*t} values over arid and semi-arid regions of China are around 0.3~0.5m/s (Wang et al., 2009). Wu et al. (2013) summarized that u_{*t} range from 0.34~0.69m/s over East Asia and indicated that u_{*t} calculated by Zender et al. (2003) are relatively lower, ranging from 0.2m/s to 0.25m/s. It is apparent that modeled u_{*t} are greatly increased in the revised simulation, which is much closer to the observed values. This improvement is mainly attributed to the update of Z_0 and Z_{0s}. Comparisons between the modeled averaged PM_{10} concentrations and the observational values in four sites show that PM_{10} levels simulated by Sen_all are closer to observations than many other cases. In summary, Sen_all shows the better agreement with the observations in terms of u_{*t} and PM_{10} concentrations.

3.2 Comparison between the improved scheme and the original scheme with observations

In order to validate the model performance of the improved scheme, time series of the observed surface PM_{10} concentrations are compared against the modeled values from Control (the original scheme) and Sen_all (the improved version) during a dust episode from 27 March to 2 April of 2015 over northern China. The intensity and evolution of this dust event has been described by Wang et al. (2017), illustrating that dust particles were mainly emitted from Mongolia and Inner Mongolia province of China and a dust backflow event took place over North China on March 29. Fig. 8 compares the hourly modeled PM_{10} concentrations and observed values for nine selected sites (locations shown in Fig. S4), which are closer to the dust sources or severely affected by the dust event. It shows that the dust concentrations are generally underestimated in Control run, particularly when dust concentrations are quite high, indicating that the original scheme has difficulty in accurately reproducing the dust emission process. Sen_all generally reproduce the PM_{10} levels better than Control run. Both the magnitude and the temporal evolution of PM_{10} concentrations are captured in Sen_all quite well, with peak values much closer to the observations. Among these sites, Sen_all shows better performance over North China, e.g., Beijing, Tianjin and Huhehaote. But both Control run and Sen_all fail to capture the peak values from 29 March to 30 March. During this period, dust particles, mixed with anthropogenic pollutants, flew back due to the south wind over North China (Wang et al., 2017). Uncertainties in the meteorological field and dust heterogeneous reactions in the model may cause the model bias.

For specific periods, however, modeled peak values of some sites occur earlier (several hours) than the observations at some sites (e.g., Beijing and Tianjin in 28 March), which could be considered as a result from the uncertainty in the wind field used in the model. It shows that the surface wind is stronger in the model than the observations (Fig. S3), which may lead to stronger transport of the dust from source regions to downwind areas such as Beijing, Tianjin and Kuele. Instead, modeled and observed peak values of some sites in the source regions (e.g., Huhehaote, Xilinguole and Hami) almost simultaneously occur.

In order to quantify the performance of the model result, some statistical parameters, including the mean values, correlation coefficient (R), mean bias (MB), normalized mean bias (NMB), are calculated and listed in this paper. The statistical performance for the modeled surface PM_{10} concentrations from Control run and Sen_all against observations are presented in Table 4. It shows that dust concentrations at all selected sites are significantly underestimated in Control run, especially over northwest regions, with the MB and NMB values ranging from -163.5μg m^{-3} to -503.61μg m^{-3} and -64.61% to -68.48% respectively. It is obvious that Sen_all with updated modification greatly improves the dust concentration prediction, with mean values more comparable to the observations, and the average MB and NMB values reduce from -196.29 μg m^{-3} and -52.79% in Control run to -47.72 μg m^{-3} and -22.46% respectively. The largest improvement occurs at northwest stations (e.g. Hami, Akesu and Kuele), which are located close to Taklimakan desert. Over other regions, such as North China (e.g., Beijing, Tianjin, Huhehaote and Xilinguole), the model performance of Sen_all are slightly better than Control run.

Although the MB and NMB values of most stations are generally lower and the mean values are much closer to observation for Sen_all simulation, i.e., modifications included improve the underestimation in Control run to some extent, the dust concentrations are still generally underestimated. For stations closer to Gobi desert, such as Xilinguole, Jiuquan and Baiyin, dust concentrations are greatly underestimated with NMB<-30%, which is likely due to the uncertainty in the erodibility factor over Gobi desert used in our study (Ginoux et al., 2001). Similarly, Su and Fung (2015) evaluated the performance of dust emission schemes in WRF-Chem over East Asia, pointing out that the erodibility factor from Ginoux et al. (2001) over the Gobi desert is significantly underestimated, which may result in the underestimation of the dust emission over the Gobi desert. Given that simulated dust emission flux is directly scaled by erodibility factor, we suggest that the erodibility factor used in our model needs to be updated or improved.

As stated above, although the model can capture the overall temporal variations of surface dust concentrations, the occurrence of modeled peak values show earlier (about six hours) than the observations over several stations, which may be attributed to strong transport due to stronger surface wind used in the model. It should be noted here that this model bias contributes a lot to the simulation error, leading to smaller R and greater MB, NMB values. R values will be greatly improved if this bias is eliminated, implying that the input assimilated meteorological field is important for dust emission simulation and needs to be further evaluated and adjusted.

The averaged modeled surface PM_{10} concentrations with and without the modifications (Sen_all and Control run respectively) and observational values at ~1400 stations over China during the study period are compared in Fig. 9. It shows that dust concentrations are generally underestimated in Control run (NMB=-16%, regression slope=0.4), which could be attributed to the crude representation of soil properties, roughness length and other related elements. Incorporating improvements in scheme makes the modeling result much closer to the observations, with R values increasing from 0.6 to 0.7, NMB values changing from -16% to -11%, regression slope ranging from 0.4 to 0.6. However, the improved model still tends to underestimate the dust concentrations. Unrealistic soil properties (e.g., soil texture; roughness length) and

https://doi.org/10.5194/acp-2020-984
Preprint. Discussion started: 29 October 2020

insufficiently accurate potential source map (the erodibility factor) used to scale dust emission flux could be the possible causes.

To further investigate the model performance, spatial distributions of averaged simulated surface PM_{10} concentrations from Control run and Sen_all and their comparisons against observations are presented in Fig. 10. Results show that both Control run and Sen_all can reproduce the pattern of dust concentrations in the study region, with high values located over northwest China, North China and some areas of northeast China, indicating that GEOS-Chem can represent the main features of dust emission and transport during the dust storm. It is found that for most sites in Control run, the simulated magnitude are close to the observational values, but are underestimated over northwest China (where Gobi and Taklimakan deserts are located) and North China plain. The simulated values from Sen_all are generally larger than Control run, and are more consistent with measurements both in magnitude and in area extent, especially over the desert region of northwest China. However, dust concentrations are still underestimated over North China plain, possibly due to outdated source map or some potential dust source regions over Inner Mongolia are not well included. In addition, missing mechanism of secondary aerosol source in the model such as heterogeneous reactions could also cause the model bias (Zheng et al., 2015; Cheng et al., 2016).

Fig. 11 shows the spatial distribution of simulated averaged AOD from Control run and Sen_all as well as MODIS AOD for the study period. For better comparison, simulated AOD at 13:00 local time (Aqua passage time) are extracted. Result shows that Control run reproduces the major regions with high AOD values, e.g., eastern China, but with lower magnitude. Control run also fails to capture the high-AOD area over the Taklimakan desert, while Sen_all could capture it. Compared with Control run, Sen_all generally reproduce the spatial coverage and magnitude of the observed AOD.

3.3 Discussion

In our study, we point out that the erodibility factor (S) in the model may introduce uncertainty in modeled dust concentrations, especially over Gobi desert. Several studies indicated that S from Ginoux et al.(2001) over the Gobi Desert has been significantly underestimated and needs to be improved (Su and Fung, 2015; Zeng et al., 2020). Wu and Lin (2014) have demonstrated that the potential source regions in the southeast of Mongolia and the middle-east of Inner Mongolia are not well characterized by the S from GOCART scheme, which results in the underestimation of dust concentration in this area and its downwind regions. In addition, the source function may not provide precise enough information about the recent expansion of dust source areas over northern China, with the desertification and deforestation (Ku and Park, 2013). Studies have demonstrated that implementing a physically based parameterization instead of an empirical dust source function which is usually time-invariant and lacks physical treatment (Kok et al., 2014a, 2014b), or adopting the dynamic dust source function (Xi et al., 2015), could improve the representation of dust emission. Therefore, the dust source function should be precisely established with new updates and higher resolution using various measurements.

In terms of sandblasting efficiency α, many modeling studies as well as observational analysis have investigated its magnitude and expression, but the results may vary greatly (Kang et al., 2011; Ma et al., 2019). The formulation for α used in our improved scheme is based on LS99, which establishes the relationship between α and u_*, along with other soil-related parameters dependent on soil textures. In this study, we derived α for different soil types based on the reported values, but uncertainties still remain due to limited available measurements. In addition to the expression from MB95 and LS99, there are other α formulations proposed by Shao et al. (1996) (Shao96) and Shao04. Different from the empirical function, expressions of Shao96 and Shao04 are more sophisticated, which is the function of u_{*t} and u_* respectively, along with some size information of soil particles. Comparisons of different formulations of α for different soil types (Kang et al., 2011; Ma et al., 2019) have shown that the variation in α can reach up to several orders of magnitude, and few equations could reproduce the measured positive correlation between α and u_*, suggesting that α for different soil texture should be further investigated and observed to improve the model accuracy.

In this study, surface conditions including erodibility factor, soil texture, clay content and surface roughness length

https://doi.org/10.5194/acp-2020-984
Preprint. Discussion started: 29 October 2020

play a significant role in improving the model performance of u_*, u_{*t} and F. We conclude that substituting globally fixed values of these properties with more realistic and physical-based ones could reduce the model uncertainty and improve the understanding of dust emission mechanism. In physically-based scheme, the importance of accurate input surface properties, including soil particle size distribution (Darmenova et al., 2009; Kok, 2011a, 2011b), soil texture (Shao et al., 2011; Foroutan et al., 2017), surface roughness length (Darmenova et al., 2009; Kontos et al., 2018) and soil plastic pressure (Lu and Shao, 1999; Kang et al., 2011), have also been highlighted by many studies. Therefore, accurate and abundant observation data of soil-related properties are urgently needed, particularly over dust source region. Moreover, various and comprehensive observation methods (e.g., experimental data, field and satellite observations) are recommended in order to correct and update the input data.

4 Summary and Conclusion

In this study, we revised the treatments of dust emission processes by considering the effect of soil moisture, surface roughness, soil texture, as well as Owen effect and more physically-based formulation of sandblasting efficiency in GEOS-Chem version 12.6.0, in order to improve dust simulation over China. Several sensitivity simulations were conducted during a severe dust storm between March 27, 2015 to April 2, 2015 over northern China to analyze the effects of these modifications on u_*, u_{*t} and emission flux.

In the improved scheme, we substituted global constant value of Z_0, assumed M_{clay} in the original version with geographical variation map obtained from the measurement provided by Prigent et al. (2005) and Shangguan et al. (2014) respectively. Z_{0s} and sandblasting efficiency were calculated with formulations based on soil texture data from FAO dataset, which is more physically-based than the original version. In addition, Owen effect and drag partition correction factor were considered in the improved version.

Sensitivity result showed that the modified f_d and f_w by inclusion of the updated Z_0, Z_{0s} and M_{clay} resulted in significant alteration in u_{*t} (ranging from -8%~72%) over China. u_{*t} was increased when including the drag partition effect, particularly with the updated Z_0 and Z_{0s} field (increased by 10%~60%), which induced the modeled u_{*t} much closer to the measurements. Considering Owen effect increased modeled u_* by 0%~39%, especially over northwest China where surface wind is strong. In general, modeled u_* was increased by 5%~50% over most parts of China due to the inclusion of Owen effect and updated Z_0. In terms of sandblasting efficiency, it was decreased by 50% on average with the updated u_*-dependent-ratio following LS99, with the largest reduction occurring over regions with sand texture. Due to the combined effect of updated treatments, emission flux simulated by improved scheme was generally decreased over northern China, except in some regions of northwest China, where Owen effect played a dominant role. Better agreement between the improved model results and observational values was achieved in terms of the u_{*t} and surface PM_{10} concentrations in selected typical sites over northern China.

Compared with both surface PM_{10} observations and MODIS AOD, the revised dust emission scheme produced better performance in both temporal and spatial variation. Result showed that the dust concentrations were generally underestimated at selected sites in the original scheme, particularly when dust concentrations were high. For the improved scheme, both the magnitude and the temporal evolution of PM_{10} concentrations were well captured, with peak values much closer to the observations. According to the statistics, with the implementation of the updates, averaged PM_{10} values at selected sites were more comparable to the observations, and the average MB and NMB values were reduced from -196.29μg m^{-3} and -52.79% in Control run to -47.72μg m^{-3} and -22.46% respectively. However, for some sites closer to Gobi desert, dust concentrations were still underestimated, which was likely attributed to the uncertainty in the erodibility factor over Gobi desert. Comparison of the model results and observed averaged PM_{10} concentrations at ~1000 stations showed that the revised scheme improved the model performance, with R values increasing from 0.6 to 0.7, NMB values changing from -16% to -11%. Moreover, the improved scheme demonstrated better performance in reproducing the spatial distribution of AOD than the original scheme, particularly over the desert region of northwest China.

In summary, this study indicated that compared to the original scheme, the revised dust emission scheme had an overall better agreement with the measurements. However, more physically-based schemes and more detailed up-to-date input parameters should be further investigated and observed to improve the accuracy of model.

Code and data availability: Measurements used in this work have been listed in Sect. 2.4 and acknowledgements. For the model outputs and codes can be accessed by contacting Rong Tian (rongtian@nuist.edu.cn).

Competing interests. The authors declare that they have no conflict of interest.

Author contributions. RT designed and conducted the model experiments, analyzed the result and wrote the paper. XYM supervised the project, proposed scientific suggestions and revised the paper. JQZ processed the observation data.

Acknowledgements. This study is supported by the National Natural Science Foundation of China grants (41675004 & 41975002), the National Key R&D Program of China grants (2019YFA0606802 & 2016YFA0600404), and the Postgraduate Research & Practice Innovation Program of Jiangsu Province (grant no. SJKY19_0962). We are thankful to C. Prigent for kindly providing the input map of global surface aerodynamic roughness length Z_0; to Shangguan W. for providing the soil clay content data, which is available from the website of Land-Atmospheric Interaction Research Group at Beijing Normal University (http://globalchange.bnu.edu.cn/research/soilw#download); to Sujan Koirala for providing global soil texture map which can be downloaded at the website (http://hydro.iis.u-tokyo.ac.jp/~sujan/research/gswp3/soil-texture-map.html). We are also grateful to GEOS-Chem Support Team for their management and maintenance of GEOS-Chem model. We acknowledge to NASA, Chinese Ministry of Environmental Protection and Chinese National Meteorological Center for providing the MODIS datasets, surface PM_{10} observations and meteorological measurements respectively.

Reference:

Alfaro, S. C. and Gomes, L.: Modelling mineral aerosol production by wind erosion: Emission intensities and aerosol size distributions in source areas, J. Geophys. Res., 106, 18075–18084, 2001.

Astitha, M., Lelieveld, J., Abdel Kader, M., Pozzer, A. and de Meij, A.: Parameterization of dust emissions in the global atmospheric chemistry-climate model EMAC: impact of nudging and soil properties, Atmos. Chem. Phys., 12(22), 11057–11083, doi:10.5194/acp-12-11057-2012, 2012.

Bonan, G. B., A land surface model (LSM version 1.0) for ecological, hydrological, and atmospheric studies: Technical description and user’s guide, Tech. Rep. NCAR TN – 417+STR, Natl. Cent. for Atmos. Res., Boulder, Colo., 1996.

Chen, L., Gao, Y., Zhang, M., Fu, J. S., Zhu, J., Liao, H., Li, J., Huang, K., Ge, B., Wang, X., Lam, Y. F., Lin, C.-Y., Itahashi, S., Nagashima, T., Kajino, M., Yamaji, K., Wang, Z. and Kurokawa, J.: MICS-Asia III: multi-model comparison and evaluation of aerosol over East Asia, Atmos. Chem. Phys., 19(18), 11911–11937, doi:10.5194/acp-19-11911-2019, 2019.

Chen, S., Huang, J., Qian, Y., Zhao, C., Kang, L., Yang, B., Wang, Y., Liu, Y., Yuan, T., Wang, T., Ma, X. and Zhang, G.: An overview of mineral dust modeling over East Asia, J Meteorol Res, 31(4), 633–653, doi:10.1007/s13351-017-6142-2, 2017.

Chen, S., Zhao, C., Qian, Y., Leung, L. R., Huang, J., Huang, Z., Bi, J., Zhang, W., Shi, J., Yang, L., Li, D. and Li, J.: Regional modeling of dust mass balance and radiative forcing over East Asia using WRF-Chem, Aeolian Research, 15, 15–30, doi:10.1016/j.aeolia.2014.02.001, 2014.

Cheng, T., Peng, Y., Feichter, J. and Tegen, I.: An improvement on the dust emission scheme in the global aerosol-climate model ECHAM5-HAM, Atmos. Chem. Phys., 13, 2008.

Cheng, Y., Zheng, G., Wei, C., Mu, Q., Zheng, B., Wang, Z., Gao, M., Zhang, Q., He, K., and Carmichael, G.: Reactive nitrogen chemistry in aerosol water as a source of sulfate during haze events in China, Science Advances, 2, e1601530, https://doi.org/10.1126/sciadv.1601530, 2016.

Chin, M., Diehl, T., Tan, Q., Prospero, J. M., Kahn, R. A., Remer, L. A., Yu, H., Sayer, A. M., Bian, H., Geogdzhayev, I. V., Holben, B. N., Howell, S. G., Huebert, B. J., Hsu, N. C., Kim, D., Kucsera, T. L., Levy, R. C., Mishchenko, M. I., Pan, X., Quinn, P. K., Schuster, G. L., Streets, D. G., Strode, S. A., Torres, O., and Zhao, X.-P.: Multi-decadal aerosol variations from 1980 to 2009: a perspective from observations and a global model, Atmos. Chem. Phys., 14, 3657–3690, https://doi.org/10.5194/acp-14-3657-2014, 2014.

Darmenova, K., Sokolik, I. N., Shao, Y., Marticorena, B., and Bergametti, G.: Development of a physically based dust emission module within the Weather Research and Forecasting (WRF) model: Assessment of dust emission parameterizations and input parameters for source regions in Central and East Asia, J. Geophys. Res., 114, D14201, doi:10.1029/2008JD011236, 2009.

DeMott, P. J., Sassen, K., Poellot, M. R., Baumgardner, D., Rogers, D. C., Brooks, S. D., Prenni, A. J., and Kreidenweis, S. M. African dust aerosols as atmospheric ice nuclei, Geophys. Res. Lett., 30, 1732, doi:10.1029/2003gl017410, 2003.

DeMott, P. J., Prenni, A. J., Liu, X., Kreidenweis, S. M., Petters, M. D., Twohy, C. H., Richardson, M. S., Eidhammer, T., and Rodgers, D. C.: Predicting global atmospheric ice nuclei distributions and their impacts on climate, P. Natl. Acad. Sci. USA, 107, 11217–11222, 2010.

Fairlie, T. D., Jacob, D. J., and Park, R. J.: The impact of transpacific transport of mineral dust in the United States, Atmos. Environ., 41, 1251–1266, 2007.

Fecan, F., Marticorena, B., and Bergametti, G.: Parametrization of the increase of the aeolian erosion threshold wind friction velocity due to soil moisture for arid and semi-arid areas, Ann. Geophys., 17, 149–157, doi:10.1007/s00585-999-0149-7, 1999.

Foroutan, H., Young, J., Napelenok, S., Ran, L., Appel, K. W., Gilliam, R. C. and Pleim, J. E.: Development and evaluation of a physics-based windblown dust emission scheme implemented in the CMAQ modeling system: WINDBLOWN DUST IN CMAQ, J. Adv. Model. Earth Syst., 9(1), 585–608, doi:10.1002/2016MS000823, 2017.

Gherboudj, I., Beegum, S. N., Marticorena, B. and Ghedira, H.: Dust emission parameterization scheme over the MENA region: Sensitivity analysis to soil moisture and soil texture: DUST EMISSION OVER MENA REGION, J. Geophys. Res. Atmos., 120(20), 10,915-10,938, doi:10.1002/2015JD023338, 2015.

Giannadaki, D., Pozzer, A., and Lelieveld, J.: Modeled global effects of airborne desert dust on air quality and premature mortality, Atmos. Chem. Phys., 14, 957–968, https://doi.org/10.5194/acp-14-957-2014, 2014.

Gillette, D. A., Fryrear, D. W., Gill, T. E., Ley, T., Cahill, T. A., and Gearhart, E. A.: Relation of vertical flux of particles smaller than 10 μm to total aeolian horizontal mass flux at Owens Lake, J. Geophys. Res.-Atmos., 102, 26009–26015, https://doi.org/10.1029/97JD02252, 1997.

Ginoux, P., Chin, M., Tegen, I., Prospero, J. M., Holben, B., Dubovik, O. and Lin, S.-J.: Sources and distributions of dust aerosols simulated with the GOCART model, J. Geophys. Res., 106(D17), 20255–20273, doi:10.1029/2000JD000053, 2001.

Ginoux, P., Prospero, J. M., Torres, O., and Chin, M.: Long-term simulation of global dust distribution with the GOCART model: correlation with North Atlantic Oscillation, Environmental Model. Soft., 19, 113–128, 2004.

Gomes, L., Arrúe, J. L., López, M. V., Sterk, G., Richard, D., Gracia, R., Sabre, M., Gaudichet, A. and Frangi, J. P.: Wind erosion in a semiarid agricultural area of Spain: the WELSONS project, CATENA, 52(3–4), 235–256, doi:10.1016/S0341-8162(03)00016-X, 2003.

Goudie, A. S.: Desert dust and human health disorders, Environ. Int., 63, 101–113, https://doi.org/10.1016/j.envint.2013.10.011, 2014.

Huneeus, N., Schulz, M., Balkanski, Y., Griesfeller, J., Prospero, J., Kinne, S., Bauer, S., Boucher, O., Chin, M., Dentener, F., Diehl, T., Easter, R., Fillmore, D., Ghan, S., Ginoux, P., Grini, A., Horowitz, L., Koch, D., Krol, M. C., Landing, W., Liu, X., Mahowald, N., Miller, R., Morcrette, J.-J., Myhre, G., Penner, J., Perlwitz, J., Stier, P., Takemura, T., and Zender, C. S.: Global dust model intercomparison in AeroCom phase I, Atmos. Chem. Phys., 11, 7781–7816, doi:10.5194/acp-11-7781-2011, 2011.

Iversen, J. D. and White, B. R.: Saltation threshold on Earth, Mars and Venus, Sedimentology, 29(1), 111–119, doi:10.1111/j.1365-3091.1982.tb01713.x, 1982.

Ju, T., Li, X., Zhang, H., Cai, X., and Song, Y.: Comparison of two different dust emission mechanisms over the Horqin Sandy Land area: Aerosols contribution and size distributions, Atmos. Environ., 176, 82–90, https://doi.org/10.1016/j.atmosenv.2017.12.017, 2018.

Kang, J.-Y., Yoon, S.-C., Shao, Y. and Kim, S.-W.: Comparison of vertical dust flux by implementing three dust emission schemes in WRF/Chem, J. Geophys. Res., 116(D9), D09202, doi:10.1029/2010JD014649, 2011.

Klingmüller, K., Metzger, S., Abdelkader, M., Karydis, V. A., Stenchikov, G. L., Pozzer, A. and Lelieveld, J.: Revised mineral dust emissions in the atmospheric chemistry–climate model EMAC (MESSy 2.52 DU_Astitha1 KKDU2017 patch), Geosci. Model Dev., 11(3), 989–1008, doi:10.5194/gmd-11-989-2018, 2018.

Kok, J. F.: Does the size distribution of mineral dust aerosols depend on the wind speed at emission?, Atmos. Chem. Phys., 11, 10149–10156, doi:10.5194/acp-11-10149-2011, 2011a.

Kok, J. F.: A scaling theory for the size distribution of emitted dust aerosols suggests climate models underestimate the size of the global dust cycle, Proc. Natl. Acad. Sci. USA, 108, 1016–1021, 2011b.

Kok, J. F., Mahowald, N. M., Fratini, G., Gillies, J. A., Ishizuka, M., Leys, J. F., Mikami, M., Park, M.-S., Park, S.-U., Van Pelt, R. S. and Zobeck, T. M.: An improved dust emission model – Part 1: Model description and comparison against measurements, Atmos. Chem. Phys., 14(23), 13023–13041, doi:10.5194/acp-14-13023-2014, 2014a.

Kok, J. F., Albani, S., Mahowald, N. M. and Ward, D. S.: An improved dust emission model – Part 2: Evaluation in the Community Earth System Model, with implications for the use of dust source functions, Atmos. Chem. Phys., 14(23), 13043–13061, doi:10.5194/acp-14-13043-2014, 2014b.

Kontos, S., Liora, N., Giannaros, C., Kakosimos, K., Poupkou, A. and Melas, D.: Modeling natural dust emissions in the central Middle East: Parameterizations and sensitivity, Atmospheric Environment, 190, 294–307, doi:10.1016/j.atmosenv.2018.07.033, 2018.

Ku, B. and Park, R. J.: Comparative inverse analysis of satellite (MODIS) and ground (PM10) observations to estimate dust emissions in East Asia, Asia-Pacific J Atmos Sci, 49(1), 3–17, doi:10.1007/s13143-013-0002-5, 2013.

Kumar, R., Barth, M. C., Pfister, G. G., Naja, M., and Brasseur, G. P.: WRF-Chem simulations of a typical premonsoon dust storm in northern India: influences on aerosol optical properties and radiation budget, Atmos. Chem. Phys., 14, 2431–2446, https://doi.org/10.5194/acp-14-2431-2014, 2014.

Latimer, R.N.C., and R.V. Martin, Interpretation of measured aerosol mass scattering efficiency over North America using a chemical transport model, Atmos. Chem. Phys., 19, 2635-2653, 2019.

Laurent, B., Marticorena, B., Bergametti, G., Chazette, P., Maignan, F., and Schmechtig, C.: Simulation of the mineral dust emission frequencies from desert areas of China and Mongolia using an aerodynamic roughness length map derived from the POLDER/ADEOS-1 surface products, J. Geophys. Res., 110, D18S04, doi:10.1029/2004JD005013, 2005.

Laurent, B., Marticorena, B., Bergametti, G., and Mei, F.: Modeling mineral dust emissions from Chinese and Mongolian deserts, Global Planet. Changes, 52, 121–141, 2006.

Laurent, B., Marticorena, B., Bergametti, G., Leon, J.-F., and Mahowald, N.: Modeling mineral dust emissions from the Sahara desert using new surface properties and soil database, J. Geoo99phys. Res., VOL. 113, D14218, doi:10.1029/2007JD009484, 2008.

Liu, D., Ishizuka, M., Mikami, M., and Shao, Y.: Turbulent characteristics of saltation and uncertainty of saltation model parameters, Atmos. Chem. Phys., 18, 7595–7606, https://doi.org/10.5194/acp-18-7595-2018, 2018.

Liu, H., Jacob, D. J., Bey, I., and Yantosca, R. M.: Constraints from 210Pb and 7Be on wet deposition and transport in a global three-dimensional chemical tracer model driven by assimilated meteorological fields, J. Geophys. Res., 106, 12109–12128, doi:10.1029/2000JD900839, 2001.

Lu, H. and Shao, Y.: A new model for dust emission by saltation bombardment, J. Geophys. Res., 104(D14), 16827–16842, doi:10.1029/1999JD900169, 1999.

Ma, S., Zhang, X., Gao, C., Tong, D. Q., Xiu, A., Wu, G., Cao, X., Huang, L., Zhao, H., Zhang, S., Ibarra-Espinosa, S., Wang, X., Li, X. and Dan, M.: Multimodel simulations of a springtime dust storm over northeastern China: implications of an evaluation of four commonly used air quality models (CMAQ v5.2.1, CAMx v6.50, CHIMERE v2017r4, and WRF-Chem v3.9.1), Geosci. Model Dev., 12(11), 4603–4625, doi:10.5194/gmd-12-4603-2019, 2019.

Macpherson, T., Nickling, W. G., Gillies, J. A. and Etyemezian, V.: Dust emissions from undisturbed and disturbed supply-limited desert surfaces, J. Geophys. Res., 113(F2), F02S04, doi:10.1029/2007JF000800, 2008.

Mahowald, N. and Kiehl, L.: Mineral aerosol and cloud interactions, Geophys. Res. Lett., 30, 1475, doi:10.1029/2002GL016762, 2003.

Marticorena, B. and Bergametti, G.: Modeling the atmospheric dust cycle: 1. Design of a soil-derived dust emission scheme, J. Geophys. Res., 100(D8), 16415, doi:10.1029/95JD00690, 1995.

Menut, L., Pérez, C., Haustein, K., Bessagnet, B., Prigent, C. and Alfaro, S.: Impact of surface roughness and soil texture on mineral dust emission fluxes modeling: IMPACT OF ROUGHNESS AND SOIL TEXTURE ON MINERAL DUST, J. Geophys. Res. Atmos., 118(12), 6505–6520, doi:10.1002/jgrd.50313, 2013.

Mokhtari, M., Gomes, L., Tulet, P. and Rezoug, T.: Importance of the surface size distribution of erodible material: an improvement on the Dust Entrainment And Deposition (DEAD) Model, Geosci. Model Dev., 5(3), 581–598, doi:10.5194/gmd-5-581-2012, 2012.

Nagashima, K., Suzuki, Y., Irino, T., Nakagawa, T., Tada, R., Hara, Y., Yamada, K. and Kurosaki, Y.: Asian dust transport during the last century recorded in Lake Suigetsu sediments, Geophys. Res. Lett., 43(6), 2835–2842, doi:10.1002/2015GL067589, 2016.

Owen, P. R., Saltation of uniform grains in air, J. Fluid Mech., 20, 225–242, 1964.

Panebianco, J. E., Mendez, M. J. and Buschiazzo, D. E.: PM10 Emission, Sandblasting Efficiency and Vertical Entrainment During Successive Wind-Erosion Events: A Wind-Tunnel Approach, Boundary-Layer Meteorol, 161(2), 335–353, doi:10.1007/s10546-016-0172-7, 2016.

Perlwitz, J. P., Pérez García-Pando, C., and Miller, R. L.: Predicting the mineral composition of dust aerosols – Part 1: Representing key processes, Atmos. Chem. Phys., 15, 11593–11627, https://doi.org/10.5194/acp-15-11593-2015, 2015a.

Perlwitz, J. P., Pérez García-Pando, C., and Miller, R. L.: Predicting the mineral composition of dust aerosols – Part 2: Model evaluation and identification of key processes with observations, Atmos. Chem. Phys., 15, 11629–11652, https://doi.org/10.5194/acp-15-11629-2015, 2015b.

Prigent, C., Tegen, I., Aires, F., Marticorena, B., and Zribi M.: Estimation of the aerodynamic roughness length in arid and semiarid regions over the globe with the ERS scatterometer, J. Geophys. Res., 110, D09205, doi:10.1029/2004JD005370, 2005.

Prigent, C., Jiménez, C. and Catherinot, J.: Comparison of satellite microwave backscattering (ASCAT) and visible/near-infrared reflectances (PARASOL) for the estimation of aeolian aerodynamic roughness length in arid and semi-arid regions, Atmos. Meas. Tech., 5(11), 2703–2712, doi:10.5194/amt-5-2703-2012, 2012.

Rajot, J. L., Alfaro, S. C., Gomes, L. and Gaudichet, A.: Soil crusting on sandy soils and its influence on wind erosion, CATENA, 53(1), 1–16, doi:10.1016/S0341-8162(02)00201-1, 2003.

Ridley, D. A., Heald, C. L., and Ford, B.: North African dust transport and deposition: a satellite and model perspective, J. Geophys. Res., 117, D02202, doi:10.1029/2011JD016794, 2012.

Ridley, D. A., Heald, C. L., Kok, J. F. and Zhao, C.: An observationally constrained estimate of global dust aerosol optical depth, Atmos. Chem. Phys., 16(23), 15097–15117, doi:10.5194/acp-16-15097-2016, 2016.

Roney, J. A. and White, B. R.: Estimating fugitive dust emission rates using an environmental boundary layer wind tunnel, Atmospheric Environment, 40(40), 7668–7685, doi:10.1016/j.atmosenv.2006.08.015, 2006.

Saidou Chaibou, A. A., Ma, X. and Sha, T.: Dust radiative forcing and its impact on surface energy budget over West Africa, Sci Rep, 10(1), 12236, doi:10.1038/s41598-020-69223-4, 2020a.

Saidou Chaibou, A. A., Ma, X., Kumar, K. R., Jia, H., Tang, Y. and Sha, T.: Evaluation of dust extinction and vertical profiles simulated by WRF-Chem with CALIPSO and AERONET over North Africa, Journal of Atmospheric and Solar-Terrestrial Physics, 199, 105213, doi:10.1016/j.jastp.2020.105213, 2020b.

Shangguan, W., Dai, Y., Duan, Q., Liu, B. and Yuan, H.: A global soil data set for earth system modeling, J. Adv. Model. Earth Syst., 6(1), 249–263, doi:10.1002/2013MS000293, 2014.

Shao, Y.,: A model for mineral dust emission, J. Geophys. Res., 106, 20239–20254, https://doi.org/10.1029/2001JD900171, 2001.

Shao, Y.,: Simplification of a dust emission scheme and comparison with data, J. Geophys. Res., 109, D10202, https://doi.org/10.1029/2003JD004372, 2004.

Shao, Y., Ishizuka, M., Mikami, M., and Leys, J. F.: Parameterization of size-resolved dust emission and validation with measurements, J. Geophys. Res., 116, D08203, doi:10.1029/2010JD014527, 2011.

Shao, Y. P., Raupach, M. R., and Leys, J. F.: A model for predicting aeolian sand drift and dust entrainment on scales from paddock to region, Austr. J. Soil Res., 34, 309–342, 1996.

Su, L. and Fung, J. C. H.: Sensitivities of WRF-Chem to dust emission schemes and land surface properties in simulating dust cycles during springtime over East Asia: Simulated Dust Cycles Over East Asia, J. Geophys. Res. Atmos., 120(21), 11,215-11,230, doi:10.1002/2015JD023446, 2015.

Tegen, I., A. L. Andrew, and I. Fung, The influence on climate forcing of mineral aerosols from disturbed soils, Nature, 380, 419–422, 1996.

Tegen, I., Harrison, S. P., Kohfeld, K., Prentice, I. C., Coe, M., and Heimann, M.: Impact of vegetation and preferential source areas on global dust aerosol: Results from a model study, J. Geophys. Res.-Atmos., 107, 4576, doi:10.1029/2001JD000963, 2002.

Tegen, I.: Modeling the mineral dust aerosol cycle in the climate system, Quaternary Sci. Rev., 22, 1821–1834, 2003.

Tian, R., Ma, X., Jia, H., Yu, F., Sha, T. and Zan, Y.: Aerosol radiative effects on tropospheric photochemistry with GEOS-Chem simulations, Atmospheric Environment, 208, 82–94, doi:10.1016/j.atmosenv.2019.03.032, 2019.

Todd, M. C., Bou Karam, D., Cavazos, C., Bouet, C., Heinold, B., Baldasano, J. M., Cautenet, G., Koren, I., Perez, C., Solmon, F., Tegen, I., Tulet, P., Washington, R., and Zakey, A.: Quantifying uncertainty in estimates of mineral dust flux: an intercomparison of model performance over the Bodele Depression, Northern Chad, J. Geophys. Res., 113, D24107, doi:10.1029/2008JD010476, 2008.

Tong, D. Q., Wang, J. X. L., Gill, T. E., Lei, H., and Wang, B.: Intensified dust storm activity and Valley fever infection in the southwestern United States, Geophys. Res. Lett., 44, 4304–4312, https://doi.org/10.1002/2017GL073524, 2017.

Uno, I., Wang, Z., Chiba, M., Chun, Y. S., Gong, S. L., Hara, Y., Jung, E., Lee, S.-S., Liu, M., Mikami, M., Music, S., Nickovic, S., Satake, S., Shao, Y., Song, Z., Sugimoto, N., Tanaka, T. and Westphal, D. L.: Dust model intercomparison (DMIP) study over Asia: Overview, J. Geophys. Res., 111(D12), D12213, doi:10.1029/2005JD006575, 2006.

Wang, C. Z., Niu, S. J., and Zhou, Y.: Recent progress on the observation study of wind erosion in China, Meteorological Monthly, 11,107-116, 2009. (in Chinese)

Wang, Z., Pan, X., Uno, I., Li, J., Wang, Z., Chen, X., Fu, P., Yang, T., Kobayashi, H., Shimizu, A., Sugimoto, N. and Yamamoto, S.: Significant impacts of heterogeneous reactions on the chemical composition and mixing state of dust particles: A case study during dust events over northern China, Atmospheric Environment, 159, 83–91, doi:10.1016/j.atmosenv.2017.03.044, 2017.

Wu, C.-L.: Improvements of Dust Emission Processes in CESM Model and Its Application, doctoral dissertation. University of Chinese Academy of Sciences, 2013. (in Chinese)

Wu, C. L. and Lin Z. H.: Impact of two different dust emission schemes on the simulation of a severe dust storm in East Asia using the WRF/Chem model, Climatic and Environmental Research, 19 (4): 419-436, 2014. (in Chinese)

Wu, M., Liu, X., Yang, K., Luo, T., Wang, Z., Wu, C., Zhang, K., Yu, H. and Darmenov, A.: Modeling Dust in East Asia by CESM and Sources of Biases, J. Geophys. Res. Atmos., 124(14), 8043–8064, doi: 10.1029/2019JD030799, 2019.

Xi, X. and Sokolik, I. N.: Seasonal dynamics of threshold friction velocity and dust emission in Central Asia, J. Geophys. Res. Atmos., 120(4), 1536–1564, doi:10.1002/2014JD022471, 2015.

Zender, C. S., Bian, H., and Newman, D.: Mineral Dust Entrainment and Deposition (DEAD) model: Description and 1990s dust climatology, J. Geophys. Res., 108, 4416, doi:10.1029/2002JD002775, 2003.

Zeng, Y., Wang, M., Zhao, C., Chen, S., Liu, Z., Huang, X. and Gao, Y.: WRF-Chem v3.9 simulations of the East Asian dust storm in May 2017: modeling sensitivities to dust emission and dry deposition schemes, Geosci. Model Dev., 13(4), 2125–2147, doi:10.5194/gmd-13-2125-2020, 2020.

Zhang, L., Gong, S., Padro, J., and Barrie, L.: A size-segregated particle dry deposition scheme for an atmospheric aerosol module, Atmos. Environ., 35, 549–560, 2001.

Zhang, J., Teng, Z., Huang, N., Guo, L. and Shao, Y.: Surface renewal as a significant mechanism for dust emission, Atmos. Chem. Phys., 16(24), 15517–15528, doi:10.5194/acp-16-15517-2016, 2016.

Zhao, C., Chen, S., Leung, L. R., Qian, Y., Kok, J. F., Zaveri, R. A., and Huang, J.: Uncertainty in modeling dust mass balance and radiative forcing from size parameterization, Atmos. Chem. Phys., 13, 10733–10753, https://doi.org/10.5194/acp-13-10733-2013, 2013.

Zhao, C., Liu, X., and Leung, L. R.: Impact of the Desert dust on the summer monsoon system over Southwestern North America, Atmos. Chem. Phys., 12, 3717–3731, https://doi.org/10.5194/acp-12-3717-2012, 2012.

Zhao, J., Ma, X., Wu, S. and Sha, T.: Dust emission and transport in Northwest China: WRF-Chem simulation and comparisons with multi-sensor observations, Atmospheric Research, 241, 104978, doi:10.1016/j.atmosres.2020.104978, 2020.

Zheng, B., Zhang, Q., Zhang, Y., He, K. B., Wang, K., Zheng, G. J., Duan, F. K., Ma, Y. L., and Kimoto, T.: Heterogeneous chemistry: a mechanism missing in current models to explain secondary inorganic aerosol formation during the January 2013 haze episode in North China, Atmos. Chem. Phys., 15, 2031–2049, https://doi.org/10.5194/acp-15-2031-2015, 2015.

Table 1. Input soil aggregate size distribution parameters dependent on soil texture classification following USDA.

	Mode1			Mode2			Mode3			
Soil Texture	**n**	**MMD**	**σ**	**n**	**MMD**	**σ**	**n**	**MMD**	**σ**	Z_{0s}
Sand	0.9	1000	1.6	0.1	100	1.7	0	10	1.8	33.3
Loamy sand	0.6	690	1.6	0.3	100	1.7	0.1	10	1.8	23
Sandy loam	0.6	520	1.6	0.3	100	1.7	0.1	5	1.8	17.3
Silt loam	0.5	520	1.6	0.35	100	1.7	0.15	5	1.8	17.3
Loam	0.35	520	1.6	0.5	75	1.7	0.15	2.5	1.8	17.3
Sandy clay loam	0.3	210	1.7	0.5	75	1.7	0.2	2.5	1.8	7
Silt clay loam	0.3	210	1.7	0.5	50	1.7	0.2	2.5	1.8	7
Clay loam	0.2	125	1.7	0.5	50	1.7	0.3	1	1.8	4.2
Sandy clay	0.65	100	1.8	0	10	1.8	0.35	1	1.8	3.3
Silty clay	0.6	100	1.8	0	10	1.8	0.4	0.5	1.8	3.3
Clay	0.5	100	1.8	0	10	1.8	0.5	0.5	1.8	3.3
Silt	0.45	520	1.6	0.4	75	1.7	0.15	2.5	1.8	17.3

Including three-mode log-normal parameters (mass fraction n (%), mass median diameter MMD (μm), and geometric standard deviation σ), and smooth aeolian roughness length z_{0s} (μm).

Table 2. Input soil-related parameters for different soil texture used in calculation of sandblasting efficiency α.

Soil Texture	$p(N\,m^{-2})$	$f(\%)$	$\rho_b(\mathrm{kg}\,m^{-3})$	C_α
Sand	5000	6.9	1000	0.01
Loamy sand	5000	18.5	1000	0.008
Sandy loam	10000	22.3	800	0.7
Silt loam	10000	22.3	800	0.7
Loam	10000	22.3	800	0.7
Sandy clay loam	10000	22.3	800	0.9
Silt clay loam	10000	22.3	800	0.7
Clay loam	10000	22.3	800	0.9
Sandy clay	30000	72	700	0.2
Silty clay	30000	72	700	0.2
Clay	30000	72	700	0.2
Silt	10000	22.3	800	0.9

Table 3. Sensitivity Experiments design and description.

Experiment name	**Modifications**					**Description**
	Updated M_{clay}	**Owen effect**	**Updated α**	**Drag partition correction (Default Z_0, Z_{0s})**	**Updated Z_0, Z_{0s}**	
Control	N	N	N	N	N	Original scheme with default configurations. Serves as a control simulation.
Sen_mclay	Y	N	N	N	N	Adopting global M_{clay} from Shangguan et al. (2014).
Sen_owen	N	Y	N	N	N	Considering Owen effect.
Sen_ratio	N	N	Y	N	N	Using updated α from Lu and Shao (1999).
Sen_drag	N	N	N	Y	N	Considering f_d but with Z_0=0.01 cm, Z_{0s}=0.0033 cm
Sen_ Z_0Z_{0s}	N	N	N	N	Y	Using updated Z_0 from Prigent et al. (2005) and updated Z_{0s}.
Sen_all	Y	Y	Y	Y	Y	Improved scheme including all the modifications described above.

Table 4. Statistics for observed and simulated (Control and Sen_all) surface PM_{10} concentrations at selected sites.

Sites	**Obs mean ($\mu g\ m^{-3}$)**	**Mod mean ($\mu g\ m^{-3}$)**		**R**		**MB ($\mu g\ m^{-3}$)**		**NMB (%)**	
		Control	**Sen_all**	**Control**	**Sen_all**	**Control**	**Sen_all**	**Control**	**Sen_all**
Beijing	232.33	130.54	148.90	0.17	0.15	-87.40	-64.78	-37.62	-27.88
Tianjin	196.68	121.86	135.89	0.01	0.02	-72.87	-52.46	-37.05	-26.67
Huhehaote	148.35	108.76	119.88	0.67	0.66	-39.02	-27.49	-26.30	-18.53
Xilinguole	116.51	48.35	64.11	0.56	0.57	-72.47	-73.17	-62.20	-62.80
Kuele	487.96	163.88	559.67	0.57	0.55	-315.26	123.77	-64.61	25.37
Hami	238.74	146.58	453.88	0.64	0.81	-163.50	-50.57	-68.48	-21.18
Akesu	738.39	236.09	827.03	0.45	0.50	-503.61	79.95	-68.20	10.83
Jiuquan	653.77	320.55	464.01	0.19	0.34	-338.29	-227.17	-51.74	-34.75
Baiyin	295.84	120.45	155.93	0.46	0.69	-174.16	-137.55	-58.87	-46.50
Average	345.40	155.23	325.48	0.41	0.48	-196.29	-47.72	-52.79	-22.46

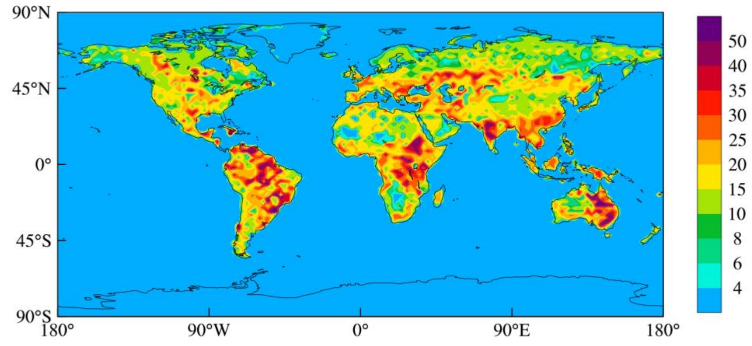

Fig 1. Updated input data of global M_{clay} (%). Data is derived from Shangguan et al. (2014) and is re-gridded to 2° × 2.5° horizontal resolution in the model.

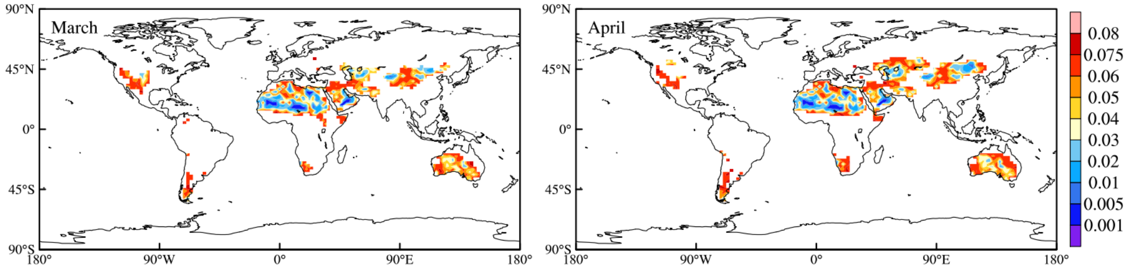

Fig 2. Monthly updated input data of global aerodynamic roughness length (Z_0) (cm) in March (left) and April (right). Data is derived from Prigent et al. (2005) and re-gridded to 2° × 2.5° horizontal resolution in the model.

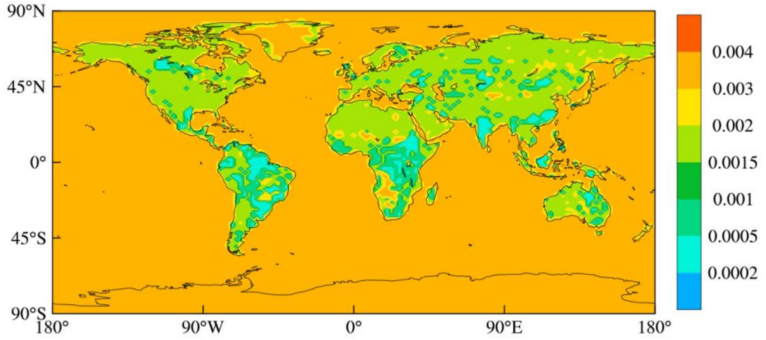

Fig 3. Updated global map of smooth roughness length (Z_{0s}) estimated from the empirical relationship with soil texture.

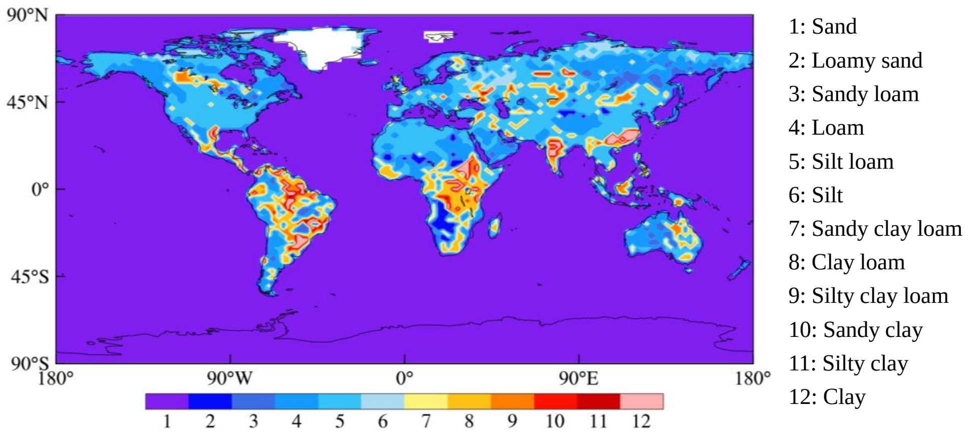

Fig 4. Global soil texture map based on the USDA classification.

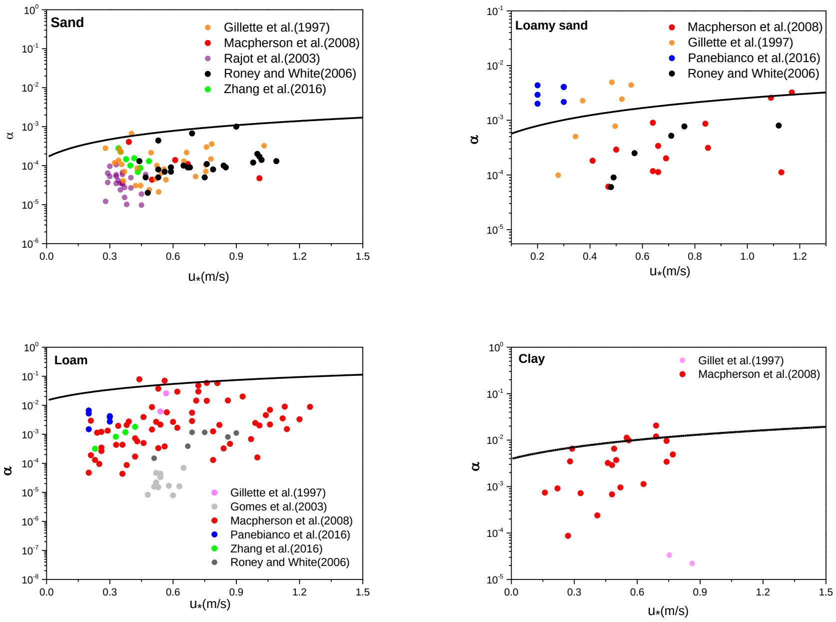

Fig 5. Updated sandblasting efficiency α as a function of surface friction velocity u_* following Lu and Shao (1999) for sand, loamy loam, loam and clay and observations from the literature.

(a) Threshold friction velocity

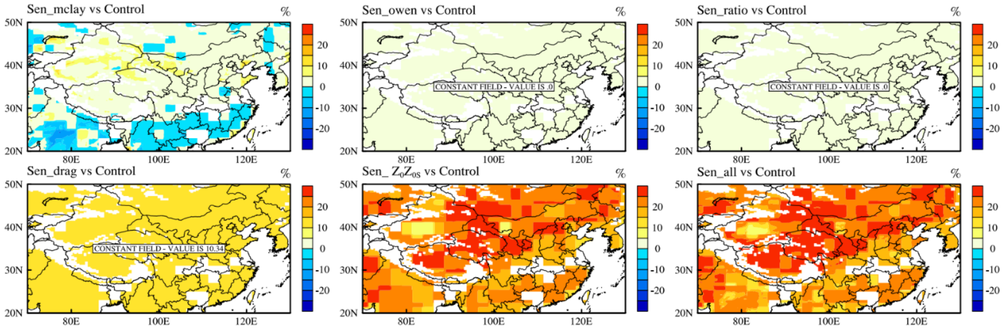

(b) Surface friction velocity

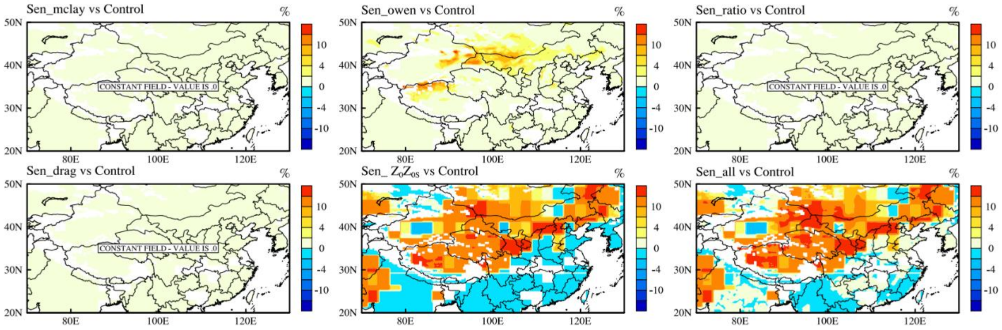

(c) Sandblasting efficiency

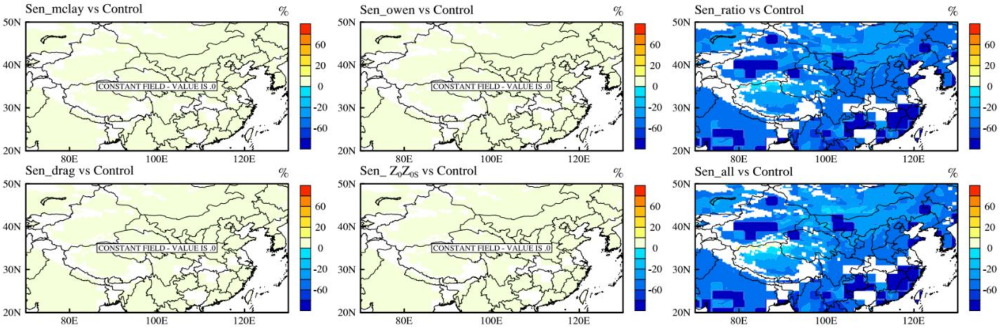

(d) Emission flux

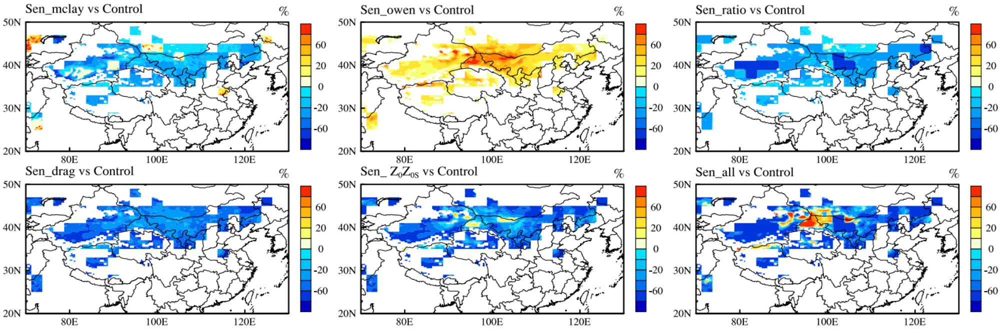

Fig 6. Relative difference (%) in simulated averaged threshold friction velocity u_{*t} (a), surface friction velocity u_*

(b), sandblasting efficiency α (c) and emission flux (d) between sensitivity simulations and control run during the study period.

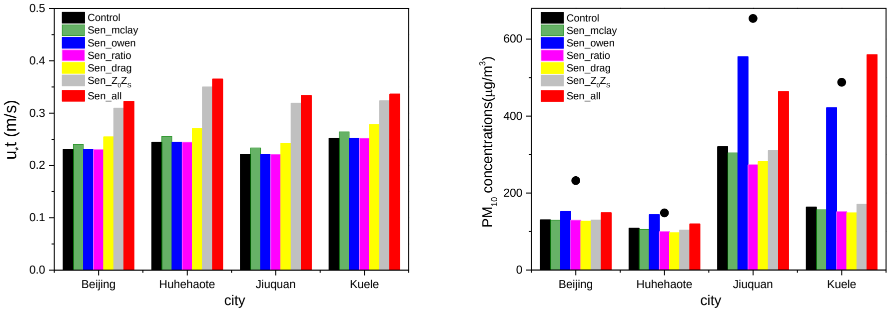

Fig 7. Comparisons of simulated averaged threshold friction velocity u_{*t} (left) and PM$_{10}$ concentrations (right) at selected sites. Black dots in right figure indicate the observed averaged PM$_{10}$ concentrations.

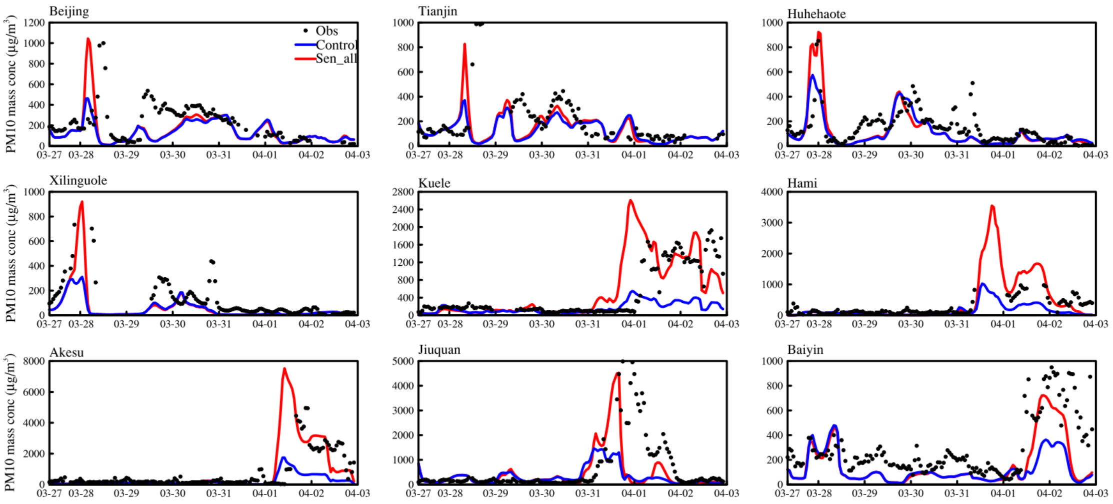

Fig 8. Temporal variation of hourly PM$_{10}$ concentrations from observations (black dots) and simulations of Control run (blue line) and Sen_all (red line) during the study period at nine selected sites.

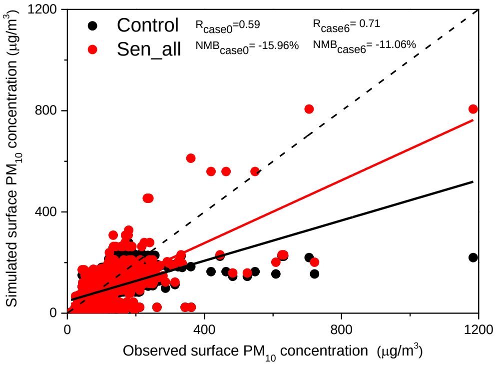

675 Fig 9. Comparison of modelled and measured surface PM_{10} concentrations at observational sites. The dotted line is
676 the 1:1 line. Model results are taken from Control run and Sen_all respectively.

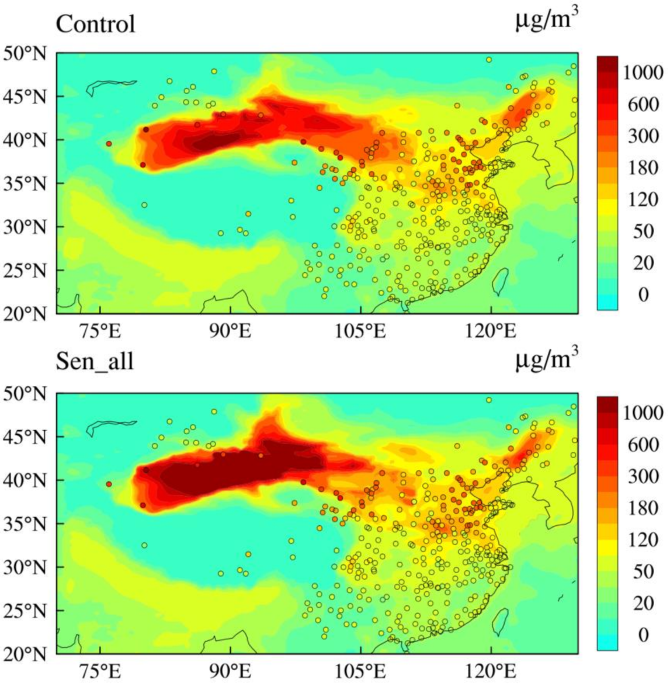

677

678 Fig 10. Comparison of simulated averaged PM_{10} surface concentrations from Control run (top) and Sen_all (bottom)
679 with the observed values.

680

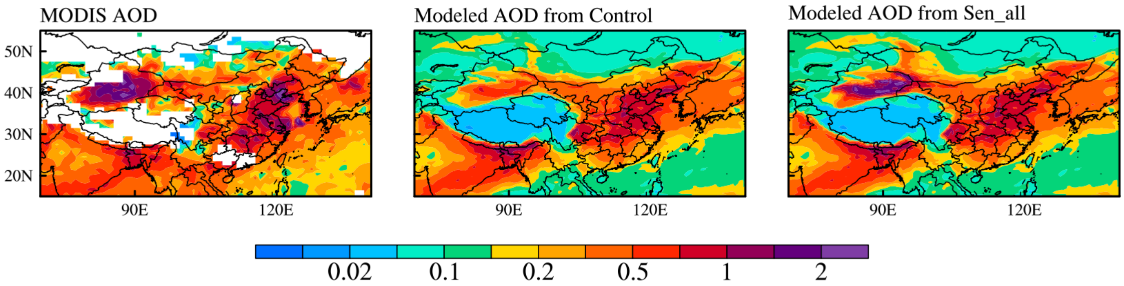

681

682 Fig 11. Spatial distribution of MODIS retrieved AOD at 550nm (left column) and simulated AOD at 550 nm from
683 Control run (middle column) and Sen_all (right column). The simulation results are extracted at 13:00 local time to
684 match the MODIS observation time.